



# Heat Transfer Analysis of Flat Plate Subjected to Multi-Jet Air Impingement using Principal Component Analysis and Computational Technique

P. Chandramohan<sup>1</sup>, S. N. Murugesan<sup>2†</sup> and S. Arivazhagan<sup>3</sup>

<sup>1</sup>*Department of Mechanical Engineering, Misrimal Navajee Munoth Jain Engineering College, Chennai, Tamil Nadu, India.*

<sup>2</sup>*Department of Mechanical Engineering, Rajalakshmi Engineering College, Chennai, Tamil Nadu, India.*

<sup>3</sup>*Department of Mechanical Engineering, St. Joseph's College of Engineering, Chennai, Tamil Nadu, India.*

†Corresponding Author Email: [murugesan.sn@rajalakshmi.edu.in](mailto:murugesan.sn@rajalakshmi.edu.in)

(Received March 25, 2016; accepted August 9, 2016)

## ABSTRACT

The aim of this work is to investigate experimentally the variation in temperature, heat transfer coefficient and Nusselt number of a hot plate subjected to multi-jet air impingement cooling to use the multi-objective optimization technique to arrive at optimum conditions. A flat plate of 15 cm x 10 cm is heated through a heating foil with a constant heat flux of 7667 W/m<sup>2</sup>. Air jets with and without swirling action are considered, fixing the distance of target surface from nozzle exit at 2D, 4D and 6D. Reynolds numbers 18000, 20000 and 22000 and pipe diameters 8mm, 10mm and 12 mm have been considered for investigation. Experiments are designed and analyzed using Taguchi's technique, coupled with principal component analysis for multi-variate optimization by calculating multi-response performance index (MRPI). Based on the observations made, it is concluded that lower H/D ratio and higher Reynolds number result in higher heat transfer coefficient, in accordance with the first principles. Heat transfer coefficient obtained for jets with swirl is compared with that of jet without swirling for the same Reynolds number and H/D ratio. Furthermore, it is concluded that introducing swirl results in increase of heat transfer coefficients for all the test conditions for 10mm and 12mm diameter jets. However for 8mm jet, introduction of swirl reduced the heat transfer rate for all the test conditions. From Analysis of Variance (ANOVA), it is found that significant contributions on outputs are due to the effect of H/D ratio and Reynolds number. Confirmation experiments with optimum condition result in improved heat transfer coefficient and Nusselt number. Numerical simulation has also been performed with the optimum condition. It is observed that the simulation results are in consistence with the experimental results.

**Keywords:** Heat transfer; Jet impingement cooling; Swirl impingement jet cooling; Principal component analysis.

## 1. INTRODUCTION

Several newer techniques developed in recent times are applied to improve the convective heat transfer for several industrial applications. Jet impingement cooling is one such technique which involves the release of a jet with high velocity from a nozzle towards the target area. This technique is adopted in several industrial processes such as annealing of metal and plastic sheets, drying of paper and textiles, cooling sensitive parts of engines of airplanes and cars, chemical vapor deposition, and more recently for cooling of laser and electronic components in order to meet the demand of compactness and high power consumption as reported by Son, *et al.* (2001), Matteo Fabbri (2004), Hyung Hee Cho, *et al.* (2011) and Ligrani (2012).

Considering its wide applications, extensive research has been performed to understand the theory and principle of heat transfer characteristics of jet impingement cooling. It is reported by Baughn, and Shimizu (1989), Lytle and Webb (1994), Elison and Webb (1994), that jet Reynolds number, jet to target spacing, turbulent intensity are the important operating parameters that decide the magnitude of the heat transfer coefficient attained. The physics of fluid flow and heat transfer phenomena, available empirical correlations with the values predicted and numerical method for computing the heat transfer coefficient for a single jet impinging on flat surface have been reported by Zuckerman and Lior (2006). Survey of outcome of several research activities was provided by Jambunathan *et al.* (1992), Viskanta (1993) and Carlomagno and Inario (2014). General observation

shows that the reducing the target distance from the jet and increasing the Reynolds number result in higher Nusselt number.

The major limitation of using single jet impingement is the steep drop in the heat transfer coefficient in the region away from the stagnation point. This behavior has been experimentally demonstrated by Katti *et al.* (2011). Lytle and Webb (1994) have observed the occurrence of secondary peak away from stagnation point at higher Reynolds number and lower jet to target spacing. However, the heat transfer coefficient falls sharply after this secondary peak. Li *et al.* (2016) investigated the fluid flow and heat transfer from a rectangular flat plane with constant uniform heat flux in laminar pulsating flow and compared with the experimental data. From their results, they found that the heat transfer enhancement is caused by the relatively low temperature gradient in the thermal boundary layer, and by the lower surface temperature in pulsating flows. In addition, the heat transfer resistance is much lower during reverse flow period than that during forward flow period

Uniformity of cooling can be approached by using an array of impinging jets when the area to be cooled is large. Study of heat transfer by multi-jet impingement cooling has also been taken up by several researchers. Heat transfer characteristics of multiple jets are different from that of a single jet. This is due to the interaction of spent air of the adjacent jets and also due to the interaction between the jets prior to impingement on the plate, as reported by Weigand and Spring (2011), Buchlin (2011). Chougule *et al.* (2011) have carried out CFD analysis of multi-jet air impingement on a flat plate and also conducted experiments to validate the CFD results. It was found that for a given Reynolds number, as observed in single jet, lower H/D resulted in higher heat transfer coefficient and higher Reynolds number yielded better heat transfer for a given H/D. It was also observed that for higher H/D, the jets in the outer rows become vibrant and do not impinge at the target as expected. Further it results in poor heat transfer coefficient due to mixing of jets before impinging on the target. Numerical simulation of three dimensional axisymmetric unsteady stagnation-point flow and heat transfer of a jet impinging on a flat plate which is moving towards the jet and away from the jet with varying velocity and acceleration has been carried out by Shokrgozar *et al.* (2016). It is observed that the velocity of the plate is more influential on the velocity and thermal boundary layers than the acceleration of the plate.

In multi-jet cooling, apart from jet to target spacing and Reynolds number, jet-to-jet spacing is also found to be an important operating parameter playing vital role in deciding the rate of heat transfer as given by Puvaneswari and Shailendhra (2016). The importance of jet-to-jet spacing has been investigated and reported by Bailey, and Bunker (2002), Aaron M Huber and Raymond Viskanta (1994). San and Chen (2014) investigated the effect jet interference on heat transfer distribution for five confined circular air jets

impinging on a flat plate. They noticed that the jet-to-jet distance appears to have more influence than the jet to target distance.

Several ways of increasing the heat transfer rate of single jet impingement have been investigated by many researchers. Attala and Salem (2013) investigated the influence of the geometry of the nozzle and showed experimentally that a square edge inlet nozzle gives higher local and average Nusselt number when compared to chamfered edge nozzle. Buchlin (2011) studied the influence of the angle of nozzle. However it has been demonstrated by several researchers that introducing swirl in the flow of the jet impingement gives better result in the improvement of overall heat transfer rate. Kinsella *et al.* (2008) have demonstrated that the local heat transfer coefficient drops at the stagnation point when swirl is introduced. However it improves the local heat transfer coefficient when we move away from the stagnation point such that it exceeds the heat transfer coefficient without swirl at location closer to 0.5D and remains higher till 2D. Beyond a distance of 2D from the stagnation point, the value is almost the same as that of nozzle without swirl. The authors have also demonstrated that the average heat transfer coefficient for an area covering five times the diameter of jets with swirl is higher compared to that without swirl.

Abrantes and Azevedo (2006) studied the fluid flow and heat transfer behavior of swirling impinging jets with a Reynolds number of 21,000 and confirmed that the presence of a swirl significantly intensified heat transfer from the wall at very small nozzle-to-plate distance ratio of  $H/D = 0.25$ . Several other authors have also investigated the effect of introducing swirl in a single jet.

However, the effect of swirl in a multi jet cooling has not been investigated extensively except the works done by Wannassi and Monnoyer (2015), Nuntadusit *et al.* (2012). Wannassi and Monnoyer have investigated flow pattern and heat transfer rate for multi jet cooling with a combination of nozzle with and without swirl. Nuntadusit *et al.* investigated the flow and heat transfer characteristics of multiple swirling impinging jets with  $3 \times 3$  in-line arrangement, on impinged surfaces with four different jet-to-jet distances ( $S/D=2, 4, 6$  and  $8$ ) at the constant nozzle-to-plate distance of 4. The swirling jets with the swirl numbers of 0.4 and conventional jets without swirl were tested and the results were compared. The experimental results showed that the jets with swirl offered higher heat transfer rate on impinged surfaces than the jets without swirl for all the tested jet-to-jet distances.

Thus it is clear when a large space is to be cooled requiring a high heat transfer rate, multi jet cooling is definitely a favorable option. But choosing with or without swirl the optimum diameter, number of nozzles, target to jet distance, jet-to-jet spacing and Reynolds number becomes increasingly complicated, Rahimi, *et al.* (2016). In this present work, an attempt has been made to obtain

**Table 1 Selected parameters for experimentation and their values**

| Parameter          | Symbol | Level 1 (-1)  | Level 2 (0) | Level 3 (+1)     |
|--------------------|--------|---------------|-------------|------------------|
| Type of movement   | A      | With swirling | -           | Without swirling |
| H/D ratio          | B      | 2D            | 4D          | 6D               |
| Reynolds No.       | C      | 18000         | 20000       | 22000            |
| Pipe Diameter (mm) | D      | 8             | 10          | 12               |

an optimum condition for cooling a 15cm x 10cm, surface with six sets of nozzle configurations for flow with and without swirl. To simplify the problem, the number of nozzles has been fixed as 4 which in turn fixes the jet to jet spacing. Keeping the target area and jet to jet spacing fixed as taken by Long and New (2015), the influence of Reynolds number, pipe diameter, and H/D and effect of swirling on the heat transfer rate, temperature and Nusselt number have been investigated.

Sheikholeslami *et al.* (2014) have investigated a convective heat transfer problem with several variable as operating parameters and used fourth order Runge–Kutta integration scheme featuring a shooting technique for obtaining the solution. In this work, analysis is carried out to achieve higher heat transfer coefficient and Nusselt number with lower temperature. Parameters selected for the experimentation based on Taguchi’s technique are given in Table 1. Taguchi technique coupled with principal component analysis for multi-variate optimization, by calculating multi-response performance index was performed to optimize the parameters as adopted by Negi and Pattamatta (2015). With the optimized conditions a confirmation experiment is performed to validate the result and compared with the results obtained from numerical simulations to ensure the consistency.

## 2. EXPERIMENTAL STUDY

Experimental set up comprises of three parts namely blower with plenum and nozzle, the heater with thermocouples and provision for varying the distance of target plate from nozzle and the Data logger with PC for measuring and storing the temperature.

### 2.1 Experimental Setup

The photographic view of experimental set up is given in Fig.1. A rectangular heating foil of size 15cm x 10cm, heating capacity of 600 Watts is sandwiched between two steel plates of same dimension and thickness of 18 mm. A dimmerstat (regulator) is used to vary the heat supplied to the heating element. The surface temperature of the top plate is measured by K-type thermocouples, which is exposed to the jets. Agilent 34972A data logger and a personal computer with required software [Bench link data logger-3] is used to measure air temperature, and the target plate temperature. Except the top surface, all the faces of the plate area

are covered with ceramic fiber of sufficient thickness to avoid heat loss. To obtain the required H/D ratio, hot plates with heating foil are placed on a stand and by using a lead screw mechanism the height can be varied. Centrifugal blower with plenum chamber was used to supply air to the jet. The purpose of the plenum chamber is to make the flow stable and free from fluctuations. A hot wire anemometer is used to measure the velocity of air in the main duct which takes air from the blower exit to the plenum chamber. Air jets of 3 different configurations viz. 8 mm, 10 mm and 12 mm diameter as shown in Fig. 2 have been used to cool the surface of the hot plate.



**Fig. 1. Photographic view of experimental setup.**

### 2.2 Experimental Procedure

After fixing a particular nozzle assembly to the plenum chamber the blower is switched on and power supply is given to heating coil through a dimmerstat to supply a constant heat flux (7667W/m<sup>2</sup>) to the heater. By adjusting the control valve, the rate of air flow is controlled until the required Reynolds number is attained. The temperatures at the fifteen points were observed periodically from a personal computer which is connected to the data acquisition system and the final readings are noted for further calculation after steady state is attained. Reynolds number of 18000, 20000 and 22000 and H/D of 2, 4 and 6 were considered for experimentation.

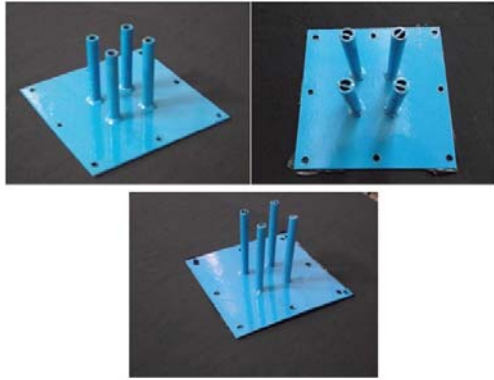


**Fig. 2. Photographic view of nozzles.**

The Nusselt number can be calculated in the numerical and experimental investigation as:

$$Nu = \frac{hD}{k} \quad (1)$$

where,

h - heat transfer coefficient, W/m<sup>2</sup> °C,

D - diameter, m,

k - thermal conductivity, W/m °C

The heat transfer coefficient can be calculated as:

$$h = \frac{q_{surface}}{T_{surface} - T_{bulk}} \quad (2)$$

where,

q - heat flux, W/m<sup>2</sup>

T - Temperature, K

### 2.3 Assumptions Made

The following assumptions are made while conducting the experiments on the flat plate.

1. The discharge is same through all the jets and their sum is equal to the flow rate of air in the main duct.
2. The temperature drop across the layer between the bead of the thermocouple and the top surface of the plate is negligible.
3. The total plate area can be divided into fifteen sub areas with one thermocouple fixed at its center. The temperature measured by each thermocouple indicates the average temperature of the respective sub area so that the average of these fifteen thermocouples indicates the average temperature of the plate.
4. Heat loss from all the faces except the top surface is negligible.

### 2.4 Experimental Uncertainty in Heat Transfer Coefficient

The heat transfer coefficient values were experimentally obtained from the rate of heat transfer per unit area and the difference in temperature between the hot plate and the ambient as given in equation (2).

The uncertainty in the value of heat transfer coefficient calculated using the above mentioned expression depends on the uncertainties in the measurement of the rate of heat transfer which in turn depends on the uncertainty of air velocity and the uncertainty in the measurement of temperature.

Using the method recommended by Holman (2004), uncertainties in the experimental heat transfer coefficient is  $\pm 5.05\%$ , computed from the uncertainty of air velocity which is given by the manufacturer as  $\pm 5\%$  and the uncertainty in the temperature measured estimated as  $\pm 0.33^\circ\text{C}$ .

## 3. OPTIMIZATION METHOD USED

### 3.1 Taguchi's Technique

Dr. Genich Taguchi philosophy in quality engineering is that, quality has to be inbuilt and designed into the product and by minimizing deviation of values from target values and performance of products be insensitive to noise factors, Roy (2001), Ross (1996). He simplified the design of orthogonal arrays (OA) with the concept of linear graph. Taguchi suggested the use of additive model and linear graphs. Additive model includes only the main effects and do not consider the interaction effects, whereas linear graph is a graphical representation of interaction information Celik and Turgut (2012). Taguchi makes use of signal to noise (S/N) ratio that combines mean and variance. S/N ratio depends on the type of quality characteristics, which are smaller the better, larger the better and nominal the better. In this work, larger the better concept is considered which is given by:

$$S / N = -10 \log \left( \frac{1}{n} \sum_{i=1}^n \frac{1}{y_i^2} \right) \quad (3)$$

The smaller the better concept considered is given by:

$$S / N = -10 \log \left( \frac{1}{n} \sum_{i=1}^n y_i^2 \right) \quad (4)$$

The parameters chosen in this work with their coded values are given in Table 1. The orthogonal array selected is of mixed level design, considering two levels for one parameter and three levels for other parameters. For this a L<sub>18</sub> (2<sup>7</sup>, 3<sup>7</sup>) orthogonal array is selected. Table 2 shows the L<sub>18</sub> orthogonal array with coded values and actual (level) values.

### 3.2 Principal Component Analysis

Factor analysis is a multi-variate technique which is applied to a set of variables when a systematic interdependence exists as proposed by Kumar and Balaji (2010), Nasser Fard, *et al.* (2016). Principal component analysis (PCA) is a multi-variate technique having a mathematical procedure, summarizing information present in the original variables in terms of smaller or newer set of uncorrelated combinations developing a minimum information loss. PCA combines variables

**Table 2 Designed L18 orthogonal array with coded and real values**

| Trial No | Coded values     |           |              |               | Actual values    |           |              |               |
|----------|------------------|-----------|--------------|---------------|------------------|-----------|--------------|---------------|
|          | Type of movement | H/D ratio | Reynolds No. | Pipe Diameter | Type of movement | H/D ratio | Reynolds No. | Pipe Diameter |
| 1        | -1               | -1        | -1           | -1            | With swirling    | 2D        | 18000        | 8             |
| 2        | -1               | -1        | 0            | 0             | With swirling    | 2D        | 20000        | 10            |
| 3        | -1               | -1        | +1           | +1            | With swirling    | 2D        | 22000        | 12            |
| 4        | -1               | 0         | -1           | -1            | With swirling    | 4D        | 18000        | 8             |
| 5        | -1               | 0         | 0            | 0             | With swirling    | 4D        | 20000        | 10            |
| 6        | -1               | 0         | +1           | +1            | With swirling    | 4D        | 22000        | 12            |
| 7        | -1               | +1        | -1           | 0             | With swirling    | 6D        | 18000        | 10            |
| 8        | -1               | +1        | 0            | +1            | With swirling    | 6D        | 20000        | 12            |
| 9        | -1               | +1        | +1           | -1            | With swirling    | 6D        | 22000        | 8             |
| 10       | +1               | -1        | -1           | +1            | Without swirling | 2D        | 18000        | 12            |
| 11       | +1               | -1        | 0            | -1            | Without swirling | 2D        | 20000        | 8             |
| 12       | +1               | -1        | +1           | 0             | Without swirling | 2D        | 22000        | 10            |
| 13       | +1               | 0         | -1           | 0             | Without swirling | 4D        | 18000        | 10            |
| 14       | +1               | 0         | 0            | +1            | Without swirling | 4D        | 20000        | 12            |
| 15       | +1               | 0         | +1           | -1            | Without swirling | 4D        | 22000        | 8             |
| 16       | +1               | +1        | -1           | +1            | Without swirling | 6D        | 18000        | 12            |
| 17       | +1               | +1        | 0            | -1            | Without swirling | 6D        | 20000        | 8             |
| 18       | +1               | +1        | +1           | 0             | Without swirling | 6D        | 22000        | 10            |

accounting for largest variance to develop the first principal component and the next largest variable accounts for second principal component, until sample variances are grouped into component groups. Multi-objective optimization problems based on Taguchi is solved with the help of Pearson (1901), Hotelling (1993) developed by means of explaining the variance-covariance structure with linear combination of measured characteristics. The PCA procedure followed in this work is similar to that used by Rajesh *et al.* (2013) as listed in the following steps:

Step 1: Developing original multiple response characteristic array

$$\begin{pmatrix} x_1(1) & x_1(2) & \dots & \dots & x_1(n) \\ x_2(1) & x_2(2) & \dots & \dots & x_2(n) \\ \vdots & \vdots & \dots & \dots & \vdots \\ \vdots & \vdots & \dots & \dots & \vdots \\ x_m(1) & x_m(2) & \dots & \dots & x_m(n) \end{pmatrix} \quad (5)$$

Where  $x_i(j)$  represents the value in the matrix,  $i = 1, 2, 3 \dots m; j = 1, 2, 3 \dots n$ . In this work,  $X$  is the normalized S/N ratio of each response and  $m=18, n=2$ .

Step 2: Evaluation of correlation coefficient array

The correlation coefficient array is evaluated as

$$R_{jl} = \left( \frac{Cov(x_i(j), x_i(l))}{\sigma_{X_i(j)} \sigma_{X_i(l)}} \right)_{j = 1, 2, 3 \dots n; l} \quad (6)$$

where,  $Cov(x_i(j), x_i(l))$  is sequence covariance of  $x_i(j)$  and  $x_i(l)$ ;  $\sigma_{x_i(j)}$  is standard deviation of  $x_i(j)$ ; sequence and  $\sigma_{x_i(l)}$  is standard deviation of  $x_i(l)$  sequence.

Step 3: Determining the eigenvectors and eigen values

From correlation array, eigenvectors and eigen values are determined.

$$(R - \lambda_k I_m) V_{ik} = 0 \quad (7)$$

where,  $\lambda_k$  eigen values

$$\sum_{k=1}^n \lambda_k = n, k = 1, 2, 3 \dots n; V_{ik} = [a_{k1} \ a_{k2} \ \dots \ a_{kn}]^T$$

eigen vectors corresponding to the eigen value  $\lambda_k$ .

Step 4: Evaluation of principal components

The formulation of uncorrelated principal component is as follows:

$$Y_{mk} = \sum_{i=1}^n X_m(i) \cdot V_{ik} \quad (8)$$

Where  $Y_{m1}$  is first principal component;  $Y_{m2}$  is second principal component, and so on. Based on variance, principal components are aligned in descending order and most of the variances in data account for first principal component.

**Table 3 Outputs measured with repeated experimental conditions**

| Trial No | Heat Transfer Coefficient |                |        | Temperature (°C) |                |       | Nusselt Number |                |        |
|----------|---------------------------|----------------|--------|------------------|----------------|-------|----------------|----------------|--------|
|          | Y <sub>1</sub>            | Y <sub>2</sub> | Y      | Y <sub>1</sub>   | Y <sub>2</sub> | Y     | Y <sub>1</sub> | Y <sub>2</sub> | Y      |
| 1        | 416.93                    | 417.23         | 417.08 | 58.86            | 56.56          | 57.71 | 142.28         | 142.78         | 142.58 |
| 2        | 513.22                    | 511.90         | 512.56 | 52.77            | 51.19          | 51.98 | 167.57         | 166.97         | 167.27 |
| 3        | 494.94                    | 495.90         | 495.42 | 51.39            | 52.13          | 51.76 | 175.95         | 175.07         | 175.51 |
| 4        | 349.92                    | 348.76         | 349.34 | 62.47            | 61.03          | 61.75 | 108.94         | 109.16         | 109.05 |
| 5        | 446.07                    | 446.75         | 446.41 | 55.61            | 54.39          | 55.00 | 142.67         | 143.19         | 142.93 |
| 6        | 419.74                    | 418.34         | 419.04 | 55.12            | 53.48          | 54.30 | 122.11         | 122.35         | 122.23 |
| 7        | 313.52                    | 314.20         | 313.86 | 62.04            | 62.82          | 62.43 | 112.43         | 111.75         | 112.09 |
| 8        | 405.91                    | 404.79         | 405.35 | 56.83            | 55.37          | 56.10 | 134.37         | 135.17         | 134.77 |
| 9        | 268.15                    | 269.51         | 268.83 | 63.42            | 62.16          | 62.79 | 102.86         | 102.16         | 102.51 |
| 10       | 418.03                    | 419.13         | 418.58 | 52.95            | 54.33          | 53.64 | 131.24         | 130.60         | 130.92 |
| 11       | 453.89                    | 454.81         | 454.35 | 54.90            | 54.38          | 54.64 | 148.31         | 147.37         | 147.84 |
| 12       | 389.34                    | 389.98         | 389.66 | 61.08            | 60.06          | 60.57 | 140.94         | 141.68         | 141.31 |
| 13       | 279.85                    | 280.45         | 280.15 | 64.83            | 65.91          | 65.37 | 99.84          | 100.26         | 100.05 |
| 14       | 397.84                    | 396.42         | 397.13 | 55.31            | 54.29          | 54.80 | 132.91         | 131.93         | 132.42 |
| 15       | 293.11                    | 291.95         | 292.53 | 56.78            | 55.64          | 56.21 | 104.97         | 103.99         | 104.48 |
| 16       | 257.48                    | 256.60         | 257.04 | 60.22            | 59.20          | 59.71 | 101.72         | 103.02         | 102.37 |
| 17       | 306.58                    | 307.18         | 306.88 | 62.56            | 64.06          | 63.31 | 119.04         | 117.88         | 118.46 |
| 18       | 263.79                    | 262.87         | 263.33 | 65.73            | 64.29          | 65.01 | 96.53          | 96.21          | 96.37  |

**4. ANALYSIS OF RESULTS**

Experiments were conducted using Taguchi’s DoE design. The output values such as heat transfer coefficient, temperature and Nusselt number were measured with repeated experimental conditions (replications) which are given in Table 3. Observations from experimental results show that, heat transfer coefficient and Nusselt number increased for all the H/D ratio with and without swirl while increasing the Reynolds number from 18000, 20000 and 22000 and pipe diameter as 8, 10 and 12 mm respectively. This result shows that increasing the Reynolds number leads to an increase in the heat transfer rate and, consequently, increases the Nusselt number. This is a general result, which holds for the flow with and without swirl. But, the measured values again decreased for Reynolds number 22000 and pipe diameter 12 mm for all the cases. Similar trend was observed by Amini *et al.* (2015), who investigated heat transfer of swirling impinging jets ejected from nozzles with twisted tapes utilizing CFD technique. The measured values again decreased for Reynolds number 22000 and pipe diameter 12 mm for all the cases. For swirl flow with H/D ratio 2D, the heat transfer coefficient increased from 417.08 to 512.56 and then decreased to 495.42. Similarly for flow without swirl and H/D ratio 6D, the heat transfer coefficient increased from 257.04 to 306.58 and then decreased to 263.33. The temperature increases linearly with increase in the Reynolds number and pipe diameter.

Because of large H/D ratio, mixing and dispersing of two sides of the jet can reduce the effect of the existence of a gap between the streams, so that the local Nusselt number was reduced for 6D H/D ratio. At a particular Reynolds number, as H/D ratio increases, the nozzle flow may mix or become wavier due to which thermal resistance of flat plate increases, which decreases the heat transfer coefficient. The higher temperature contours are observed due to cross mixing of flow and intensity of temperature zone at these area increases as we increase H/D ratio. Generally, heat transfer coefficient and Nusselt number decreases with swirling effect of jet movement and with increase in H/D ratio Celik and Turgut (2012) and increases when the pipe diameter is increased Increase in Reynolds number increases the heat transfer coefficient and Nusselt number and decreases the temperature. Significant changes in outputs are observed with change in H/D ratio and Reynolds number with introduction of swirling effect.

The following procedure is used to determine optimal input parameter combination parameters based on Taguchi’s S/N ratio combined with principal component analysis:

1. Calculation of S/N ratios for experimental results.
2. Normalization of S/N ratio values of responses.
3. Calculation of Multi-response performance index using PCA.

**Table 4 Signal-to-noise ratio and its normalized values**

| Trial No. | S/N ratio                 |             |                | Normalizing Sequence      |             |                |
|-----------|---------------------------|-------------|----------------|---------------------------|-------------|----------------|
|           | Heat Transfer Coefficient | Temperature | Nusselt Number | Heat Transfer Coefficient | Temperature | Nusselt Number |
| 1         | 52.404                    | 35.225      | 43.078         | 0.701                     | 0.534       | 0.653          |
| 2         | 54.195                    | 34.317      | 44.468         | 1.000                     | 0.982       | 0.920          |
| 3         | 53.899                    | 34.280      | 44.886         | 0.951                     | 1.000       | 1.000          |
| 4         | 50.865                    | 35.813      | 40.753         | 0.445                     | 0.244       | 0.206          |
| 5         | 52.995                    | 34.807      | 43.102         | 0.800                     | 0.740       | 0.657          |
| 6         | 52.445                    | 34.696      | 41.744         | 0.708                     | 0.795       | 0.397          |
| 7         | 49.935                    | 35.908      | 40.991         | 0.289                     | 0.197       | 0.252          |
| 8         | 52.157                    | 34.979      | 42.592         | 0.660                     | 0.655       | 0.559          |
| 9         | 48.590                    | 35.958      | 40.215         | 0.065                     | 0.172       | 0.103          |
| 10        | 52.436                    | 34.590      | 42.340         | 0.707                     | 0.847       | 0.511          |
| 11        | 53.148                    | 34.750      | 43.396         | 0.825                     | 0.768       | 0.714          |
| 12        | 51.814                    | 35.645      | 43.003         | 0.603                     | 0.327       | 0.638          |
| 13        | 48.948                    | 36.308      | 40.004         | 0.125                     | 0.000       | 0.063          |
| 14        | 51.979                    | 34.776      | 42.439         | 0.630                     | 0.756       | 0.530          |
| 15        | 49.323                    | 34.996      | 40.381         | 0.187                     | 0.647       | 0.135          |
| 16        | 48.200                    | 35.521      | 40.203         | 0.000                     | 0.388       | 0.101          |
| 17        | 49.739                    | 36.029      | 41.471         | 0.257                     | 0.137       | 0.344          |
| 18        | 48.410                    | 36.260      | 39.679         | 0.035                     | 0.024       | 0.000          |

**Table 5 Eigenvalues and variation of principal components**

| Components               | Eigenvalue | Difference | % variation | Cumulative % | Eigenvector [HTC, NN, T] |
|--------------------------|------------|------------|-------------|--------------|--------------------------|
| Z <sub>1</sub> component | 2.709      | 2.47       | 90.297      | 90.297       | [0.593, 0.556, 0.582]    |
| Z <sub>2</sub> component | 0.239      | 0.187      | 7.965       | 98.262       | [-0.272, 0.819, -0.506]  |
| Z <sub>3</sub> component | 0.052      | -          | 1.738       | 100.00       | [0.758, -0.142, -0.637]  |

4. Determination of optimal level of input parameters.
5. Adoption of ANOVA to find out the influential parameters.
6. Experiment Confirmation.

As employed by Senthilkumar *et al.* (2014), Taguchi's techniques of larger the better or smaller the better concepts, S/N ratio of outputs are determined. Heat transfer coefficient and Nusselt number should be higher whereas temperature should be lower. Table 4 shows the calculated S/N ratio. After calculating the desired S/N ratio, the values are normalized for further processing.

Principal component analysis is performed using Minitab 17 software for the output responses and the Eigen vectors and Eigen values obtained with % variation are given in Table 5, which is used for calculating the multiple response performance index Lee-Ing Tong (2005), Hung-Chang Liao (2006).

From the results of principal component analysis, the selected eigen vectors are 0.593, 0.556 and

0.582 for heat transfer coefficient, temperature and Nusselt number respectively based on the eigen value of 2.709, since a value more than 1 is desirable. Principal components for the outputs are calculated as in Table 6, considering the Square of the individual eigen values and MRPI is obtained by adding all the principal components. Based on the values of MRPI, ranking is given and the best pair of input parameters is arrived at in Experiment 3.

To determine the optimal parameter level values, the average of MRPI is calculated for each level of individual parameters as given in Table 7. Optimum condition obtained is type of movement: with swirling, H/D ratio: 2D, Reynolds No.:20000 and pipe diameter: 12 mm. Response graph of parameters and mean MRPI are drawn based on response Table 7 as in Fig. 3

Influence of one individual parameter over the other parameters can be identified with the use of interaction plots as followed Senthilkumar *et al.* (2014). If parallel graphs are obtained for change in level value of the parameters over MRPI, no

**Table 6 Principal component values for responses and MRPI**

| Trial No. | Principal Component       |             |                | Multi Response Performance Index (MRPI) | Ranking |
|-----------|---------------------------|-------------|----------------|---|---------|
|           | Heat Transfer Coefficient | Temperature | Nusselt Number |   |         |
| 1         | 0.247                     | 0.165       | 0.221          | 0.633                                   | 7       |
| 2         | 0.352                     | 0.304       | 0.312          | 0.967                                   | 2       |
| 3         | 0.334                     | 0.309       | 0.339          | 0.982                                   | 1       |
| 4         | 0.156                     | 0.075       | 0.070          | 0.302                                   | 12      |
| 5         | 0.281                     | 0.229       | 0.223          | 0.733                                   | 4       |
| 6         | 0.249                     | 0.246       | 0.134          | 0.629                                   | 8       |
| 7         | 0.102                     | 0.061       | 0.085          | 0.248                                   | 14      |
| 8         | 0.232                     | 0.203       | 0.189          | 0.624                                   | 9       |
| 9         | 0.023                     | 0.053       | 0.035          | 0.111                                   | 16      |
| 10        | 0.248                     | 0.262       | 0.173          | 0.683                                   | 5       |
| 11        | 0.290                     | 0.237       | 0.242          | 0.769                                   | 3       |
| 12        | 0.212                     | 0.101       | 0.216          | 0.529                                   | 10      |
| 13        | 0.044                     | 0.000       | 0.021          | 0.065                                   | 17      |
| 14        | 0.222                     | 0.234       | 0.180          | 0.635                                   | 6       |
| 15        | 0.066                     | 0.200       | 0.046          | 0.311                                   | 11      |
| 16        | 0.000                     | 0.120       | 0.034          | 0.154                                   | 15      |
| 17        | 0.090                     | 0.042       | 0.117          | 0.249                                   | 13      |
| 18        | 0.012                     | 0.007       | 0.000          | 0.020                                   | 18      |

**Table 7 Average MRPI values for input levels**

| Factors          | Level 1 | Level 2 | Level 3 | Max - Min | Ranking |
|------------------|---------|---------|---------|-----------|---------|
| Type of movement | 0.581   | 0.380   | -       | 0.201     | 4       |
| H/D ratio        | 0.761   | 0.446   | 0.234   | 0.526     | 1       |
| Reynolds No.     | 0.348   | 0.663   | 0.430   | 0.315     | 2       |
| Pipe Diameter    | 0.396   | 0.427   | 0.618   | 0.222     | 3       |

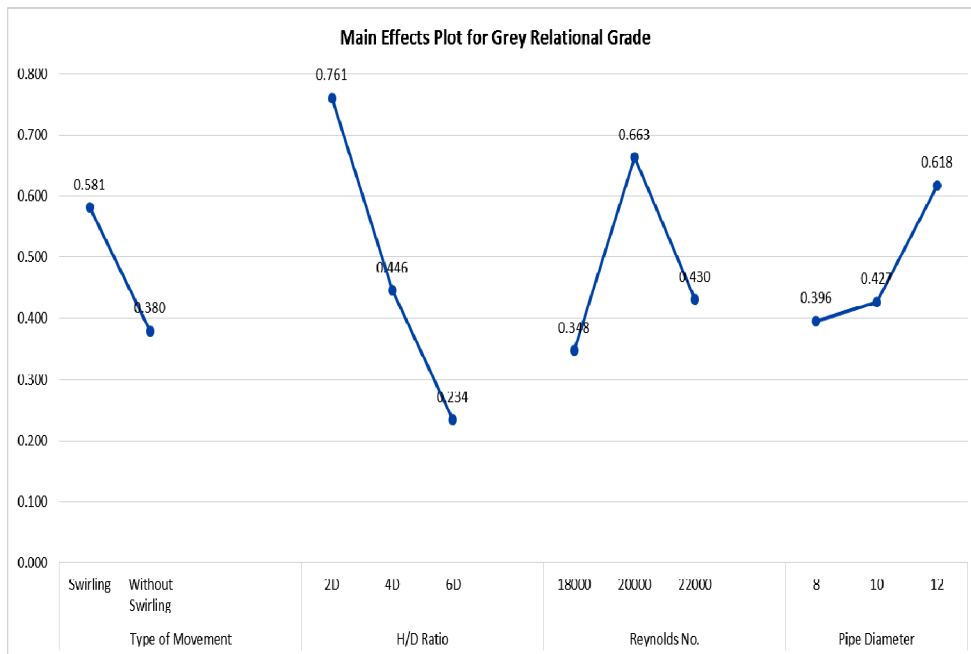


**Fig. 3. Response graph of MRPI.**

### Interaction Plot for Multi Response Performance Index

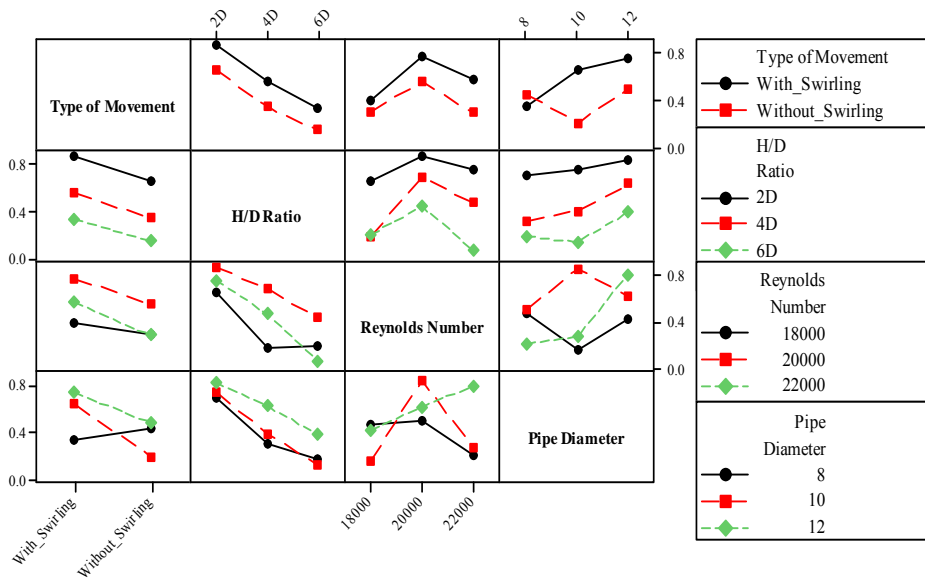


Fig. 4. Interaction effects between the input parameters and MRPI.

Table 8 ANOVA table for MRPI

| Factors          | DoF | SS     | MS     | F Value | P Value | % Contribution |
|------------------|-----|--------|--------|---------|---------|----------------|
| Type of movement | 1   | 0.1824 | 0.1824 | 39.252  | 0.000   | 11.66%         |
| H/D ratio        | 2   | 0.8416 | 0.4208 | 90.565  | 0.000   | 53.79%         |
| Reynolds No.     | 2   | 0.3206 | 0.1603 | 34.506  | 0.000   | 20.50%         |
| Pipe Diameter    | 2   | 0.1734 | 0.0867 | 18.665  | 0.000   | 11.09%         |
| Error            | 10  | 0.0465 | 0.0046 |         |         | 2.97%          |
| Total            | 17  | 1.5645 | 0.0920 |         |         | 100.00%        |

interaction exists. If non-parallel graphs are obtained, a considerable significant relationship exists. From the interaction plot of MRPI shown in Fig. 4, between type of movement and pipe diameter and also between Reynolds number and pipe diameter a relationship is seen to exist. Between other parameters no interaction effect is observed.

ANOVA and Fishers test are performed to justify the adequacy of models. When  $Prob>F$  less than 0.05, the model terms are significant due to the chosen 95% confidence interval. Values less than 0.1 are most significant as suggested by Gamst, G et.al. (2008), Montgomery, D.C. and Runger, G.C. (2011). No lack of fit is observed when the calculated values are less than the standard F ratio. Significant model terms have values less than 0.1. If standard F ratio is greater than the calculated value, then there is no lack of fit (Senthilkumar and Tamizharasan (2012). In the model, insignificant terms should be omitted based on  $R^2$  and  $R^2$  adjusted values. Table 8 shows the ANOVA results of MRPI. The obtained values of S is 0.0681635,  $R^2$  is 97.03% and  $R^2$  (adj) is 94.95% during ANOVA.

Contribution of individual parameters over the calculated MRPI is identified from the ANOVA results. Fig 5 shows the percentile contribution of each parameter over the MRPI. Higher influence of MRPI of 53.79% and 20.50% are given by H/D ratio and Reynolds Number respectively. Influence of type of movement and pipe diameter is moderate.

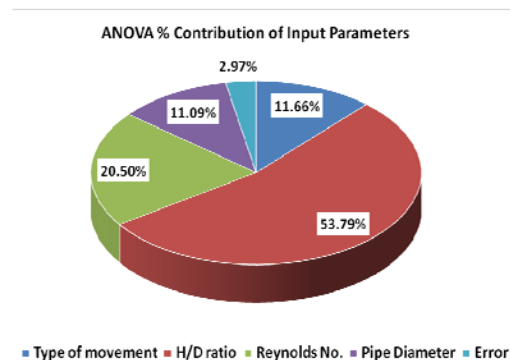
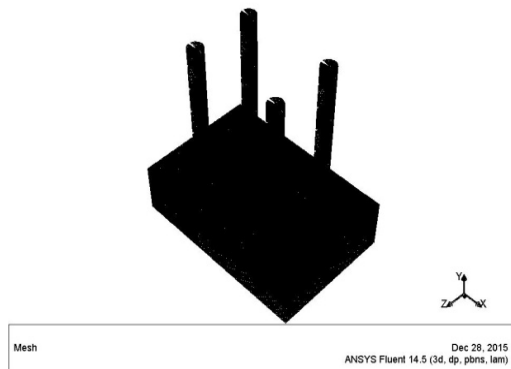


Fig. 5. Results of ANOVA showing % contribution.

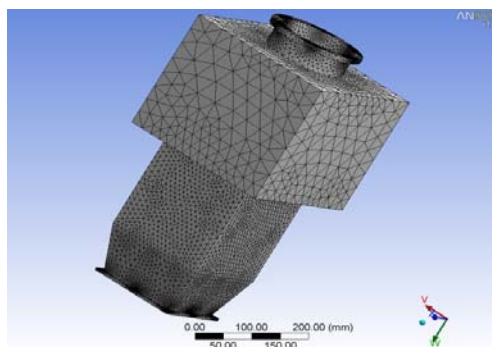
## 5. NUMERICAL SIMULATION OF HEAT TRANSFER ANALYSIS

The numerical simulations were carried out for the optimum result obtained from multi-response performance index (MRPI) as adopted by Hai-xia Liu *et al.* (2015). Figure 6 shows the finite element model of nozzle with swirl effect. Here, the flat plate attached with nozzle is discretized and meshed into small elements using tetrahedral mesh type. The details of the grid resolution study of the meshing elements are: element size is 2.32 mm in medium mesh, number of nodes is 2158385, number of elements is 8683888, tetrahedral shape of element is 7961392 and hexahedra element shape is 722496.



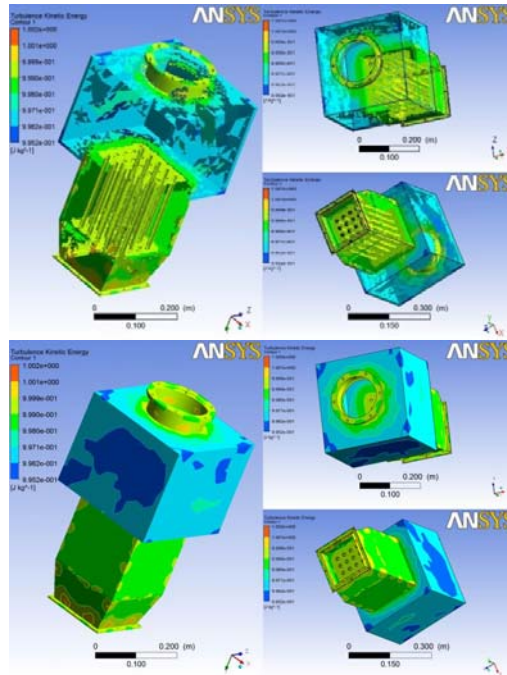
**Fig. 6. Finite element model of setup with swirling action.**

Figure 7 shows the overall meshing of plenum chamber. The mesh quality was checked by using ANSYS and the finite element analysis was carried out by Senthilkumar *et al.* (2012), Deepanraj *et al.* (2011) with  $k-\xi$  model. The following boundary conditions were used to analyze the plenum chamber with velocity of 28.88 m/sec measured from the blower outlet using hot wire anemometer.



**Fig. 7. Meshed model of plenum chamber.**

The distribution of turbulent kinetic energy of air in the plenum chamber has been computed as shown in Fig 8. It can be observed that the reduction in cross section of the plenum chamber increases the turbulence kinetic energy. The turbulent kinetic energy has increased gradually in third portion owing to the presence of an array of 25 numbers of flow regulating tubes.



**Fig. 8. Turbulent Kinetic Energy model of the plenum chamber.**

The distribution of velocity obtained from the analysis of plenum chamber and the hot plate is shown in Figs. 9 and 10 respectively. From the analysis, it is found that the velocity is uniform throughout the tube. The velocity in the tube ranges from  $2.050e+001$  to  $2.870e+001$  m/s. There is no negative velocity inside the tubes. The velocity in the plenum chamber is uniform throughout.

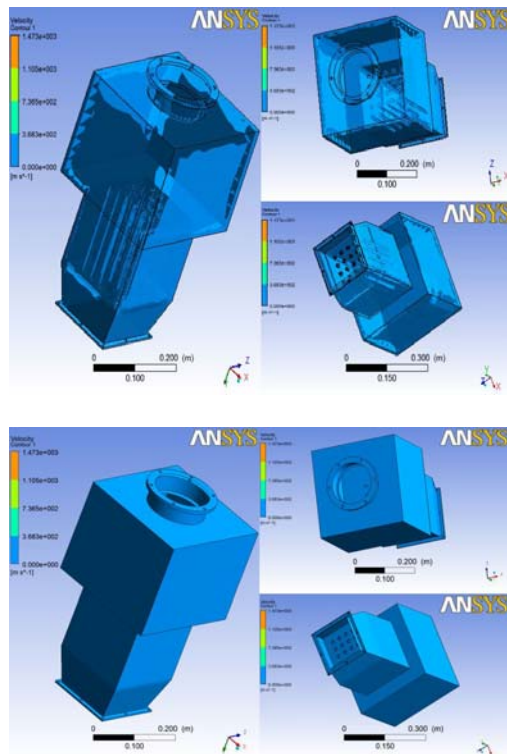


**Fig. 9. Distribution of Velocity for the plenum chamber.**

**Table 9 Comparison of experimental and FEM results**

| Sl. No | Condition             | Heat Transfer Coefficient | Temperature | Nusselt No. |
|--------|-----------------------|---------------------------|-------------|-------------|
| 1      | Experimental          | 508.35                    | 52.17       | 181.55      |
| 2      | Finite Element method | 526.40                    | 58.91       | 188.76      |
| 3      | % Error               | 3.55                      | 12.92       | 3.97        |

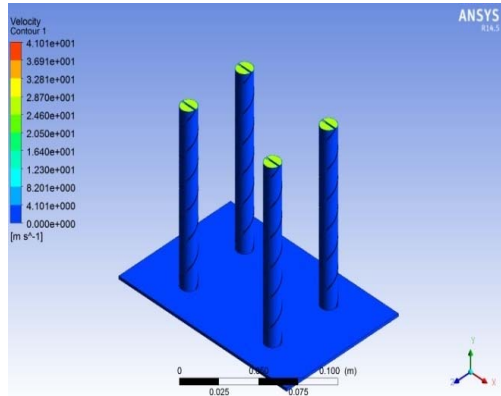


**Fig. 10. Distribution of Velocity for the tube and plate.**

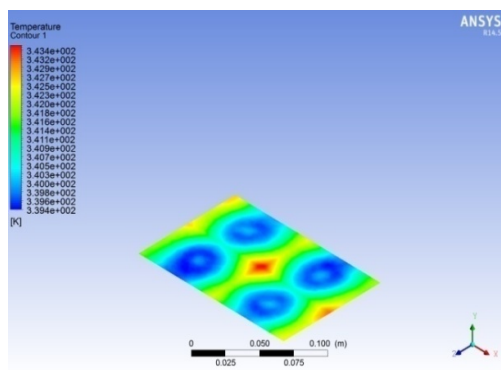
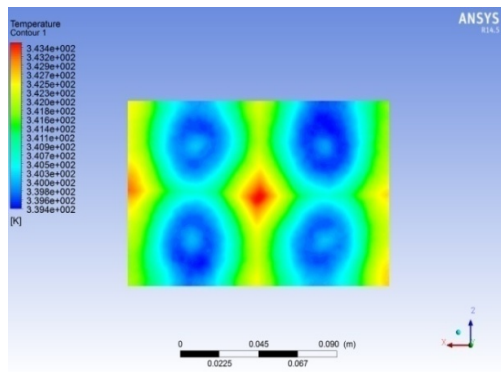


**Fig. 11. Distribution of temperature for the plate.**

cooling tubes ranges from  $3.394e+002$  to  $3.420e+002$ . As the tubes in the plate are symmetric on both X and Y axis, the temperature distribution near the tubes is same in all the four tubes. The temperature is maximum at the center of the plate as the distance between the tubes and the center of the plate is maximum. The temperature at the center of the plate is  $3.434e+002$ K. The temperature distribution obtained in simulation is compared the temperatures measured during experimentation which in turn correlates with results of Taguchi's technique.

The pressure distribution in the plenum chamber is shown in Fig. 12. Pressure is not uniform throughout the plenum chamber. Pressure is maximum in the first portion of the plenum chamber which is in the range of  $4.398e+005$ . Due to the stagnation condition, pressure in the first portion is maximum. To produce uniformity of pressure, straightening tubes were used, which reduces the pressure up to  $6.925e+004$ . Pressure distribution is uniform after flowing through the straightening tubes.

As expected the Pressure peak is higher for high Reynolds number. At any Reynolds number, the non-dimensional pressure has the highest value at the stagnation region and reduces radially. Similar trend was observed by Srivalli *et al.* (2012), who analyzed the fluid flow and heat transfer analysis of laminar multiple square jets impinging on a flat plate by varying the Reynolds number and jet to jet spacing and nozzle exit to plate distance.

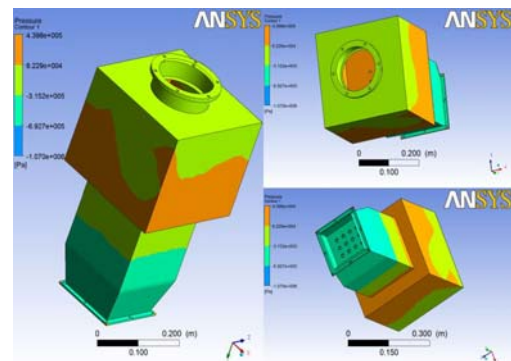


**Fig. 12. Distribution of pressure for the plenum chamber.**

The distribution of temperature in the flat plate is shown in Fig. 12. The hot plate is cooled by the air impingement passing through the cooling tubes. As the heat transfer rate is maximum at the cooling tubes section on the flat plate, temperature near the cooling tubes is minimum. The temperature in the

## 6. CONCLUSION

Experiments were conducted to determine the variation of heat transfer coefficient, temperature and Nusselt number for a hot plate subjected to

multi-jet air impingement cooling. Air jets with height to diameter (H/D) ratios of 2D, 4D and 6D, Reynolds number 18000, 20000 and 22000 and pipe diameter from 8mm, 10mm and 12 mm were taken and the best value was optimized using Taguchi's technique coupled with principal component analysis. Experiments based on swirl flow with H/D ratio of 2D, Reynold's number 20000 and pipe diameter 12 mm achieved better performance. ANOVA results of MRPI with R<sup>2</sup> value of 97.03% shows that 53.79% MRPI is influenced by H/D ratio, 20.50% by Reynolds number. Numerical simulations were performed by taking the optimized values and results compared with experimental results are very much closer to numerical results.

## REFERENCES

- Abrantes, J. K. and L. F. A. Azevedo (2006). Fluid Flow Characteristics of a Swirl Jet Impinging on a Flat Plate. In *Proceedings of the thirteenth International Symposium on Application of Laser Techniques to Fluid Mechanics*, Lisbon, Portugal.
- Amini, Y., M. Mokhtari, M. Haghshenasfard and M. B. Gerdroodbary (2015). Heat transfer of swirling impinging jets ejected from Nozzles with twisted tapes utilizing CFD technique. *Case Studies in Thermal Engineering* 6, 104-115.
- Attalla, M. and M. Salem (2013). Effect of nozzle geometry on heat transfer characteristics from a single circular air jet. *Applied Thermal Engineering* 51, 723-733.
- Bailey, J. C. and R. S. Bunker (2002). Local heat transfer and flow distributions for impinging jet arrays of dense and sparse extent. Proc. ASME TURBO EXPO, Amsterdam .
- Baughn, J. W. and S. Shimizu (1989). Heat transfer measurement from a surface with uniform heat flux and an impinging jet. *Transaction of ASME* 111, 1096-1098.
- Buchlin, J. M. (2011). Convective heat transfer in impinging- gas- jet arrangements. *Journal of Applied Fluid Mechanics* 4(2), 137-149.
- Carlmagno, G. M. and A. Ianiro (2014). Thermo-fluid-dynamics of submerged jets impinging at short nozzle-to-plate distance: a review. *Exp. Therm. and Fluid Science* 58, 15-35.
- Celik, N. and E. Turgut (2012). Design analysis of an experimental jet impingement study by using Taguchi method. *Heat Mass Transfer* 48(8), 1407-1413.
- Chougule, N. K., G. V. Parishwad, P. R. Gore, S. Pagnis and S. N. Sapali (2011). CFD analysis of multi-jet air impingement on flat plate. In *Proceeding of World Congress on Engineering, III WCE*, London.
- Deepanraj, B., P. Lawrence and G. Sankaranarayanan (2011). Theoretical analysis of gas turbine blade by finite element method. *Scientific World* 9(9), 29-33.
- Elison, B. and B.W Webb (1994). Local heat transfer to impinging liquid jets in the initially laminar, transitional, and turbulent regimes. *International Journal of Heat and Mass Transfer* 37, 1207-1216.
- Fabbri, M. (2004). *Cooling of electronic components using arrays of micro jets*. Ph. D. Thesis, University of California, Los Angeles.
- Fard N., H. Xu and Y. Fang (2016). A unique solution for principal component analysis-based multi-response optimization problems. *The International Journal of Advanced Manufacturing Technology* 82(1), 697-709.
- Gamst, G., L. S. Meyers and A. J. Guarino. (2008). *Analysis of Variance Designs - A Conceptual and Computational Approach with SPSS and SAS*. Cambridge University Press, Cambridge, U.K.
- Holman, J. P. (2004), *Experimental Methods for Engineers*. Tata McGraw-Hill.
- Hotelling, H. (1993). Analysis of a complex of statistical variables into principal components. *J. Educ. Psychol.* 24, 417-441.
- Huber, A. M. and R. Viskanta (1994). Effect of jet-jet spacing on convective heat transfer to confined, impinging arrays of axisymmetric air jets. *International Journal of Heat Mass Transfer* 37(18), 2859-2869.
- HyungHee Cho, Kyung Min Kim and Jiwoon song (2012). Applications of impingement jet cooling systems, Book chapter, pp37-68,
- Jambunathan, K., E. Lai, and M. A. Moss and B. L. Button (1992). A review of heat transfer data for single circular jet impingement. *International Journal of Heat and Fluid Flow* 13(2), 106-115.
- Jiang, F., H. Wang., Y. Wang. and J. Xiang. (2016). Simulation of flow and heat transfer of mist/air impinging jet on grinding work-piece. *Journal of Applied Fluid Mechanics* 9(3), 1339-1348.
- Katti, V. V., S. N. Ysaswy and S. V. Prabhu (2011). Local heat transfer distribution between smooth flat surface and impinging air jet from a circular nozzle at low Reynolds numbers. *Heat Mass Transfer* 47, 237-244.
- Kinsella, C., B. Donnelly1, T. S. O'Donovan and D. B. Murray (2008). Heat transfer enhancement from a horizontal surface by impinging swirl jets In *Proceeding 5th European Thermal-Sciences Conference*.
- Kumar, A. and C. Balaji (2010). A Principal Component Analysis and neural network based non-iterative method for inverse conjugate natural convection. *International Journal of Heat and Mass Transfer* 53(21-22), 4684-4695.

- Li, G., Y. Zheng, H. Yang and Y. Xu (2016). Numerical investigation of heat transfer and fluid flow around the rectangular flat plane confined by a cylinder under pulsating flow. *Journal of Applied Fluid Mechanics* 9(4), 1569-1577.
- Liao, H. C. (2006). Multi-response optimization using weighted principal component. *International Journal of Advanced Manufacturing Technology* 27, 720-725.
- Ligrani, P. (2013). Heat transfer augmentation technologies for internal cooling of turbine components of gas turbine engines. *International Journal of Rotating Machinery* 1, 1-32.
- Liu, H. X., Q. Shao, C. Kang and C. Gong (2015). Impingement capability of high-pressure submerged water jet: Numerical prediction and experimental verification. *Journal of Central South University* 22(10), 3712-3721.
- Long, J. and T. H. New (2015). A DPIV study on the effects of separation distance upon the vertical behaviour of jet-cylinder impingements. *Experiments in Fluids* 56(7), 1-21.
- Lytle, D. and B. Webb (1994). Air jet impingement heat transfer at low nozzle-plate Spacing. *International Journal of Heat Mass Transfer* 37, 1687-1697.
- Montgomery, D. C., G. C. Runger (2011). *Applied Statistics and Probability for Engineers*. John Wiley and Sons, Inc., New York.
- Negi, D. S. and A. Pattamatta (2015). Profile shape optimization in multi-jet impingement cooling of dimpled topologies for local heat transfer enhancement. *Heat and Mass Transfer* 51(4), 451-464.
- Nuntadusit, C., M. Wae-hayee, A. Bunyajitradulya, and A. Eiamsa-Ard (2012). Heat transfer enhancement by multiple swirling impinging jets with twisted-tape swirl generators. *International Communications in Heat and Mass Transfer* 39, 102-107.
- Pearson, K. (1901). On lines and planes of closest fit to systems of points in space. *Philos. Mag.* 62, 559-57.
- Puvaneswari, P. and K. Shailendra (2016). Enhancement of heat transfer in a liquid metal flow past a thermally conducting and oscillating infinite flat plate. *Journal of Applied Fluid Mechanics* 9(3), 1395-1407.
- Rahimi, M. and R. A. Soran (2016). Slot jet impingement heat transfer for the cases of moving plate and moving nozzle. *Journal of the Brazilian Society of Mechanical Sciences and Engineering* 38(8), 2651-2659.
- Rajesh, S., D. Devaraj, R. S. Pandian and S. Rajakarunakaran (2013). Multi-response optimization of machining parameters on red mud-based aluminum metal matrix composites in turning process. *International Journal of Advanced Manufacturing Technology* 67, 811-821.
- Ross, P. J. (1996). *Taguchi techniques for quality engineering: loss function, orthogonal experiments, parameter and tolerance design*. McGraw-Hill, New York.
- Roy, R. K. (2001). *Design of experiments using the Taguchi approach: 16 steps to product and process improvement*. John Wiley and Sons, USA.
- San, J. Y. and J. J. Chen (2014). Effects of jet-to-jet spacing and jet height on heat transfer characteristics of an impinging jet array. *International Journal of Heat Mass Transfer* 7(1), 8-17.
- Senthilkumar, N. and T. Tamizharasan (2012). Impact of interface temperature over flank wear in hard turning using carbide inserts. *Procedia Engineering* 38, 613-621.
- Senthilkumar, N., C. K. Dhinakaran and B. Deepanraj, N. M. Babu and A. Santhoshkumar (2012). Modification and analysis of compressor intercooler fin in turbocharger using FEM. *Procedia Engineering* 38, 379-384.
- Senthilkumar, N., T. Ganapathy, T. Tamizharasan (2014-a). Optimization of Machining and Geometrical parameters in Turning process using Taguchi Method. *Australian Journal of Mechanical Engineering* 12(2), 233-246.
- Senthilkumar, N., T. Tamizharasan and V. Anandkrishnan (2014-b). Experimental investigation and performance analysis of cemented carbide inserts of different geometries using Taguchi based grey relational analysis. *Measurement* 58, 520-536.
- Sheikholeslami M. and D. D. Ganji (2014). Heated permeable stretching surface in a porous medium using nanofluids. *Journal of Applied Fluid Mechanics* 7(3), 535-542.
- Shokrgozar, A., A. B. Rahimi and H. Mozayyeni (2016). Investigation of three-dimensional axisymmetric unsteady stagnation-point flow and heat transfer impinging on an accelerated flat plate. *Journal of Applied Fluid Mechanics* 9(1), 451-461.
- Son, C., D. Gillespie, P. Ireland and G. M. Dailey (2001). Heat transfer and flow characteristics of an engine representative impingement cooling system. *Journal of Turbomachinery* 123, 154-160.
- Srivalli, G., B. Raghavarao and M. C. Sastry, (2012). Fluid flow and heat transfer analysis of laminar multiple square jets impinging on a flat plate. *International Journal of Engineering Research and Applications* 2, 48-56.
- Tong, L. I., C. H. Wang and H. C. Chen (2005). Optimization of multiple responses using

- principal component analysis and technique for order preference by similarity to ideal solution. *International Journal of Advanced Manufacturing Technology* 27, 407-414.
- Viskanta, R. (1993). Heat transfer to impinging isothermal gas and flame jets. *Experimental Thermal Fluid Science* 6, 111-134.
- Wannassi, M. and F. Monnoyer (2015). Fluid flow and convective heat transfer of combined swirling and straight impinging jet arrays. *Applied Thermal Engineering* 78, 62-73.
- Weigand, B. and S. Spring (2011). Multiple jet impingement – a review. *Heat Transfer Research* 42(2), 101-142.
- Zuckerman, N. and N. Lior (2006). Jet impingement heat transfer: Physics, correlations, and numerical modeling. *Advances in heat transfer* 39, 565-631.